

# Automatic dataset shift identification to support root cause analysis of AI performance drift

Mélanie Roschewitz, Raghav Mehta, Charles Jones, and Ben Glocker

Imperial College London

Shifts in data distribution can substantially harm the performance of clinical AI models. Hence, various methods have been developed to detect the presence of such shifts at deployment time. However, root causes of dataset shifts are varied, and the choice of shift mitigation strategies is highly dependent on the precise type of shift encountered at test time. As such, *detecting* test-time dataset shift is not sufficient: precisely *identifying* which type of shift has occurred is critical. In this work, we propose the first unsupervised dataset shift identification framework, effectively distinguishing between prevalence shift (caused by a change in the label distribution), covariate shift (caused by a change in input characteristics) and mixed shifts (simultaneous prevalence and covariate shifts). We discuss the importance of self-supervised encoders for detecting subtle covariate shifts and propose a novel shift detector leveraging both self-supervised encoders and task model outputs for improved shift detection. We report promising results for the proposed shift identification framework across three different imaging modalities (chest radiography, digital mammography, and retinal fundus images) on five types of real-world dataset shifts, using four large publicly available datasets.

## Introduction

Machine learning models are notoriously sensitive to changes in the input data distribution, a phenomenon commonly referred to as dataset shift<sup>1–4</sup>. This is particularly problematic in clinical settings, where dataset shift is a common occurrence and may arise from various factors<sup>5</sup>. Changes in the frequency of disease positives over time or across geographical regions cause *prevalence shift*<sup>6,7</sup> (also known as label shift). The use of different acquisition protocols or scanners<sup>8–10</sup>, or a change in patient demographics<sup>11,12</sup> can induce shifts in image characteristics, known as *covariate shift*. We illustrate examples of real-world shifts in Fig. 1. Dataset shift can dramatically affect the performance of AI and lead to clinical errors such as misdiagnosis<sup>4,13,14</sup>. It is recognised as the fundamental barrier hindering AI adoption<sup>15,16</sup>. It is hence crucial to implement safeguards allowing not only effective detection of the presence of shifts, but importantly, reliable identification of the root causes. Comprehensive shift detection and identification frameworks are key for the safe deployment and continuous monitoring of AI in clinical practice.

Dataset shifts can be detected at deployment time by using statistical testing to compare the distributions of incoming test data to the distribution of the reference data (representative of the data used to validate the deployed AI model). Significant progress has been made in this field where state-of-the-art methods can detect various types of real-world shifts<sup>17–20</sup>. Shifts between test and reference data can either be detected at the output level by comparing distributions of model out-

puts, or at the input level by comparing low-dimensional feature representations of input images<sup>19</sup> (see Methods, **Dataset shift detection methods** for more details). In this study, we show that different types of shifts require different shift detection approaches. On the one hand, comparing model output distributions allows for the reliable detection of shifts directly related to the downstream task, such as changes in prevalence. On the other hand, we show that for shifts orthogonal to the downstream task, such as changes in image acquisition protocols, comparing output distributions is not sufficient. For such shifts, test and reference data need to be compared at the input level using rich feature representations. We demonstrate that self-supervised neural network image encoders<sup>21</sup>, trained without using any task-specific annotations, yield excellent low-dimensional feature representations for shift detection.

While *detecting* dataset shifts is important, it is insufficient for the safe deployment of AI. Besides knowing that there is a problem, we need to be able to *identify* its root cause to take the necessary actions, implement preventive measures, and safeguard against harm caused by AI errors. To our knowledge, no solution yet exists to identify the root cause of dataset shifts.

The precise identification of the type of shifts is critical for selecting appropriate mitigation strategies. For example, prevalence shifts can often be mitigated with lightweight output recalibration techniques<sup>14,22–24</sup>, but these rely on the assumption that no other types of shift are present. In contrast, covariate shifts require more advanced domain adaptation techniques or model fine-tuning<sup>4,25–29</sup>. The difficulty is that a change in image characteristics may cause similar changes in the distribu-

Examples of dataset shift types						
Covariate shifts						
	Acquisition shift (e.g. scanner shift)			Subpopulation shift (e.g. gender shift)	...	Prevalence shift
Source dataset	Scanner A	Scanner A	Scanner B	Female	Female	
Source dataset						
Shifted dataset						
Shifted dataset						
Shifted dataset						

**Fig. 1 Examples of dataset shifts in medical imaging. Reliably detecting and identifying the nature of the shift is crucial to enable the safe deployment of machine learning systems applications.** In this work, we propose the first shift *identification* framework able to reliably detect and classify any detected shift as (i) prevalence, (ii) covariate or (iii) mixed prevalence and covariate shift.

tion over model outputs as a change in disease prevalence<sup>4</sup>, and determining the cause of an observed shift can be challenging. Applying the wrong mitigation technique may, in the best case, be ineffective in resolving the shift or, in the worst case, severely harm model performance or calibration. In Appendix A, we show an example of the consequences of applying a prevalence shift correction algorithm to the wrong type of shift on model calibration, further motivating the need for dataset shift identification methods. Despite its paramount importance, automatic dataset shift identification has remained an open problem.

In this work, we address this issue by proposing the first dataset shift *identification* framework capable of identifying the root cause of the underlying shift, effectively separating (i) prevalence shift, (ii) covariate shift and (iii) mixed shift (both prevalence and covariate shifts). Our shift identification framework consists of two stages and is summarised in Fig. 2. First, the ‘shift detection’ module identifies whether a shift is present. Secondly, given that a shift has been detected, our ‘shift identification’ module characterises the type of shift. An in-depth evaluation across three different clinical applications (chest radiography, digital mammography, and retinal fundus images) on five types of real-world dataset shifts demonstrates that our framework accurately distinguishes between prevalence shifts, covariate shifts, and mixed shifts across various scenarios. We conclude that the proposed method may play an important role towards safe deployment and clinical adoption of medical imaging AI.

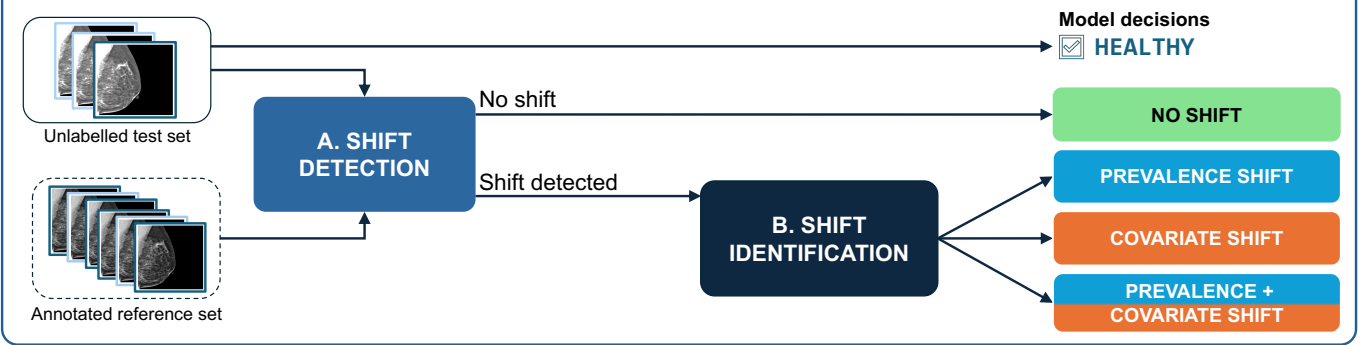
## Results

### Datasets and shift generation

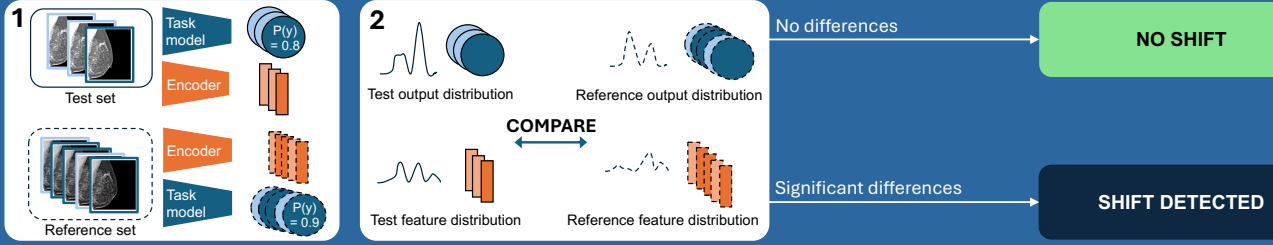
We evaluate our methods on four different datasets covering three different imaging modalities: (i) chest radiography using PadChest<sup>30</sup> and RSNA Pneumonia Detection<sup>31</sup> datasets; (ii) mammography using the EMBED<sup>32</sup> dataset, and (iii) fundus images using the Kaggle Diabetic Retinopathy Detection<sup>33</sup>, Kaggle Aptos Blindness Detection<sup>34</sup> and Messidor-v2<sup>35</sup> datasets. To study prevalence shift detection, we associate each dataset with a downstream task. For chest radiography datasets we focus on pneumonia detection (binary), for mammography on breast density assessment (4 classes), and for retinal images on diabetic retinopathy assessment (binary). More details can be found in Methods, *Datasets*.

For every dataset, we study different types of shifts at different levels of intensity. We simulate various levels of prevalence shift by resampling the test set according to specific label distributions. Similarly, we simulate different types of covariate shifts by resampling the datasets according to specific scanner, acquisition site or gender distributions. We then measure shift detection (resp. identification) accuracy by repeated sampling of shifted test sets. Specifically, for each bootstrap sample, a test set is sampled according to the defined shift generating process. We then measure how many times the shift is detected (resp. the correct shift was identified) out of all 200 bootstrap samples. Technical details on shift generation processes, experimental setup, and implementation of shift detection algorithms can be found in Methods, *Shift generation details* and

## PIPELINE OVERVIEW



### A. SHIFT DETECTION



### B. SHIFT IDENTIFICATION

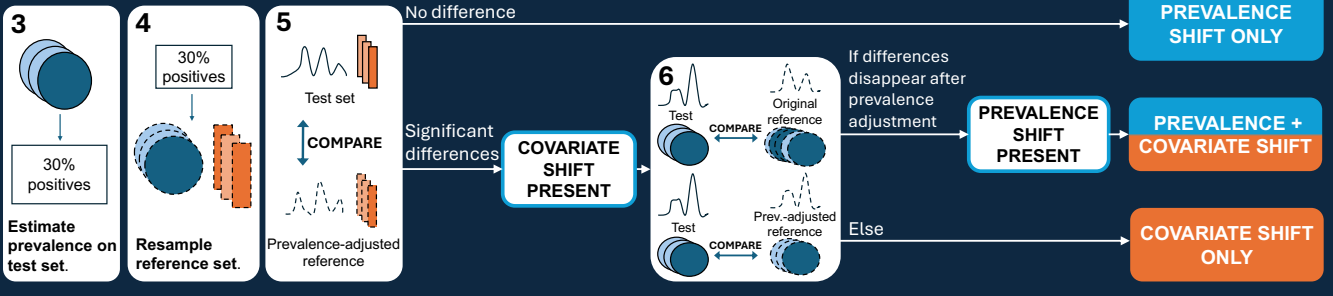


**Fig. 2 Overview of the dataset shift identification pipeline proposed in this work.** We leverage both task model outputs and features from self-supervised encoders for detecting and identifying dataset shifts. Contrarily to previous works, we do not simply detect the *presence* of shifts but also add a second step able to *identify* the nature of the shift. Our method effectively separates cases of (i) prevalence shift (a change in label distribution); (ii) covariate shift (a change in image characteristics) and (iii) covariate and prevalence shift (both). Our shift identification pipeline can be divided into two stages: (A) shift detection, followed by (B) shift identification. For shift detection, we combine signals from model outputs and generic features (low-dimensional representations of images) to detect whether a shift is present in the test set (2). If a shift is detected we proceed to shift identification. Identification starts with estimating the prevalence in the test set (3), then we resample the reference set to match the estimated test set prevalence (4). We then first compare feature distributions between prevalence-adjusted reference and test set (5): if differences are no longer significant after adjusting the prevalence, the shift is attributed to prevalence shift. Conversely, if differences persist after adjusting the prevalence, then covariate shift is necessarily present. In this case, we compare model output distributions to determine whether prevalence shift is also present (6). Precisely, if there were significant differences in model output distributions before adjusting the prevalence, but this shift disappears after adjusting the prevalence, we know that prevalence shift is also responsible for the observed shift, in this case we conclude that the observed shift is a case of mixed shift (prevalence + covariate shifts). Else, we conclude that the shift is attributed to covariate shift only.

**Implementation details.** This extensive experimental setup not only allows us to test the effectiveness of our shift identification framework but also to evaluate the sensitivity of existing dataset shift detection methods on a large variety of realistic shifts across modalities that have not been studied before in this context.

## Different shifts require different detectors

We first investigate which types of shifts are successfully detected by prominent dataset shift detection methods. We compare two families of shift detectors: model output-based and feature-based detectors leveraging representations from pretrained neural networks. We additionally propose and test a dual approach that combines both complementary approaches for improved shift detection ('Duo'). A detailed description of the shift detection tests used in this study can be found in Methods, **Dataset shift detection methods**.

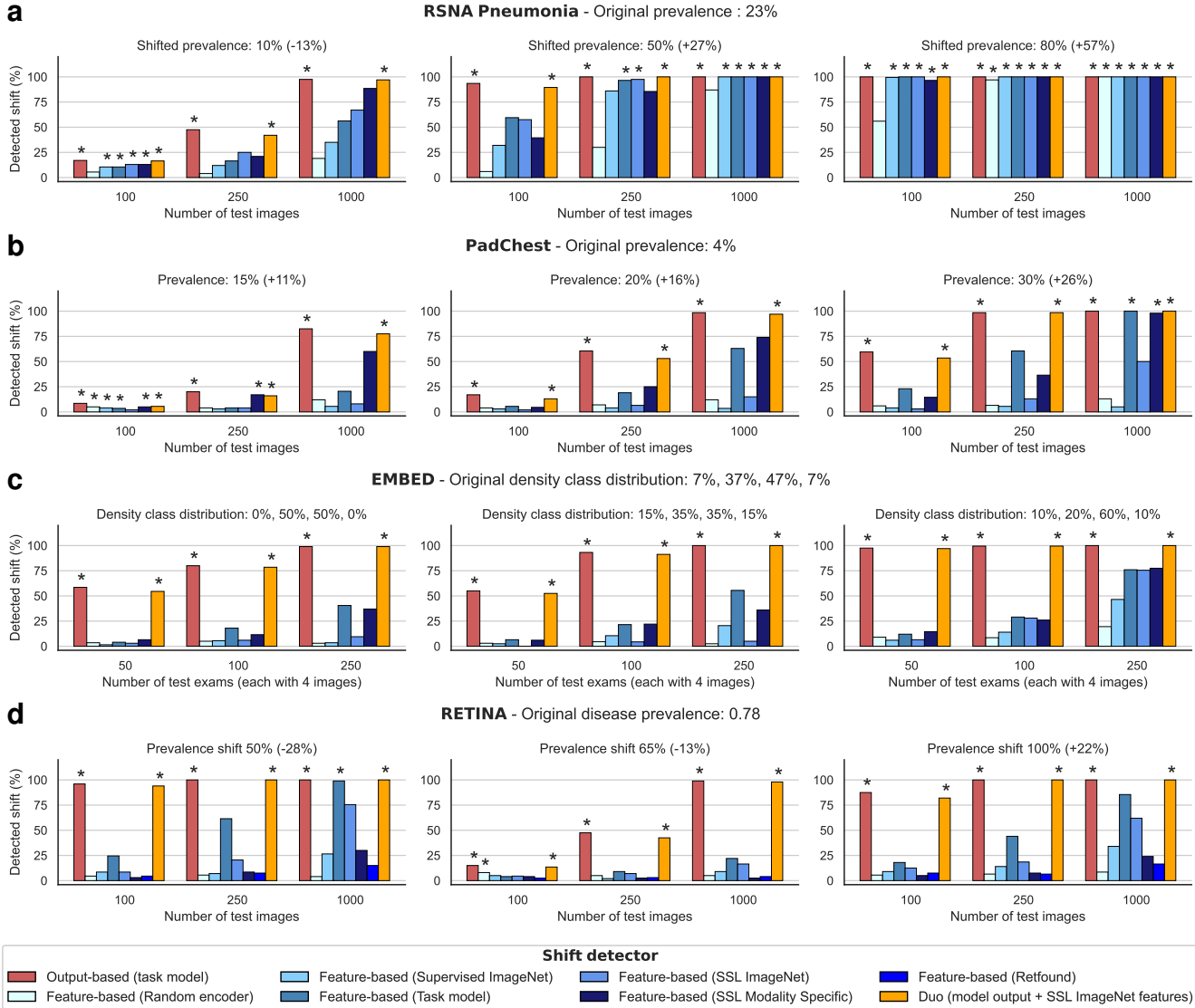
For feature-based shift detection, any pretrained network could be used as feature extractor. A perhaps obvious choice is to simply use the encoder from the task-specific classification model. However, this may not be the best choice as learned features will be heavily skewed towards encoding characteristics specifically relevant to that task as opposed to encoding more generic image representations sensitive to data distribution changes<sup>36</sup>. Hence, we here explore the potential of self-supervised (SSL) image encoders for shift detection. Indeed, encoders trained in a self-supervised manner, i.e. without any labels, learn fine-grained representations effectively summarising all the information encoded in a given image, resulting in ideal candidates for generic shift detection. We compare the performance of feature-based shift detection for five different encoders (using the features obtained from the last layer of the neural network encoder). We compare: (i) 'Random' a neural network (ResNet) encoder with random weights; (ii) 'Supervised ImageNet' where features are extracted using a ResNet encoder trained to perform classification on natural images from the ImageNet dataset; (iii) 'Task model', the ResNet encoder from the task model used to perform the downstream classification task; (iv) 'SSL ImageNet' a self-supervised encoder trained on ImageNet data only; (v) 'SSL Modality Specific' a self-supervised encoder trained on the same modality as the test datasets. Additionally, for the RETINA dataset, we include a comparison using the open-source 'RetFound'<sup>37</sup> self-supervised foundation model as a feature extractor. More details on self-supervised models can be found in Methods, **Self-supervised learning**.

**Output- and feature-based detectors detect different shifts.** Figs. 3 and 4 show the shift detection rates for every dataset-shift combination. Across all datasets, a clear pattern appears. For prevalence shifts (Fig. 3), output-based shift detection performs significantly better than all feature-based tests. This is intuitive as the shift is directly related to the downstream prediction task. A change in prevalence should directly be reflected by a change in the distribution of task model outputs. For covariate shifts, results are very different, regardless of whether

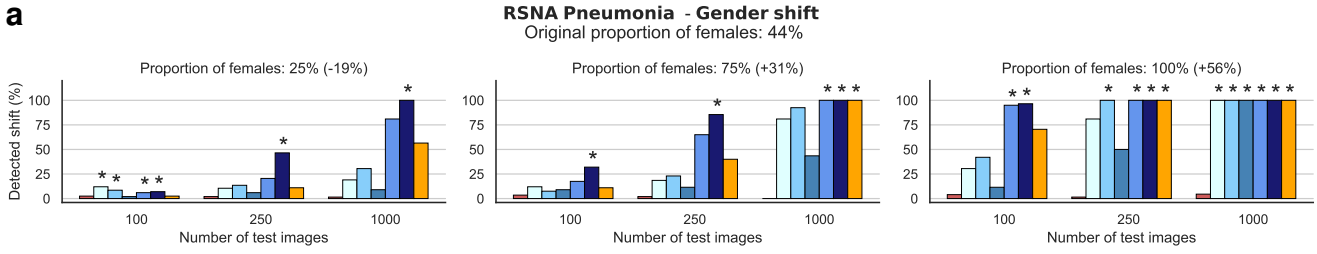
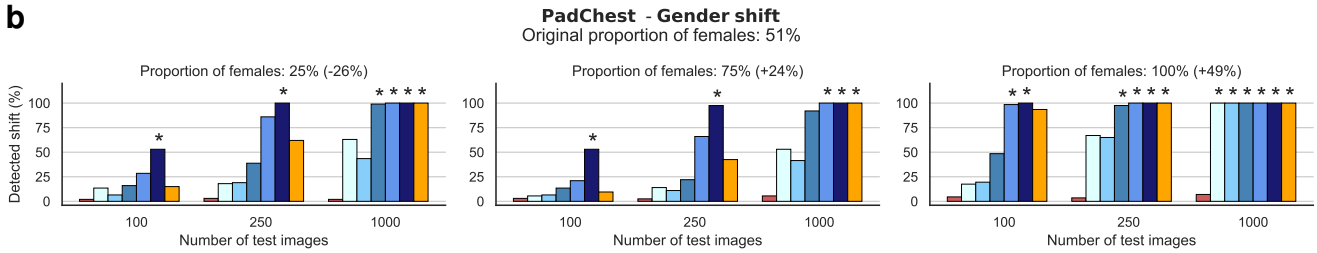
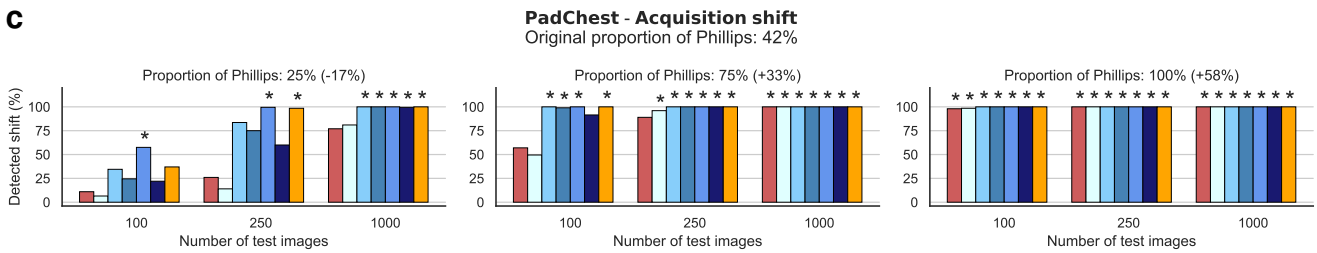
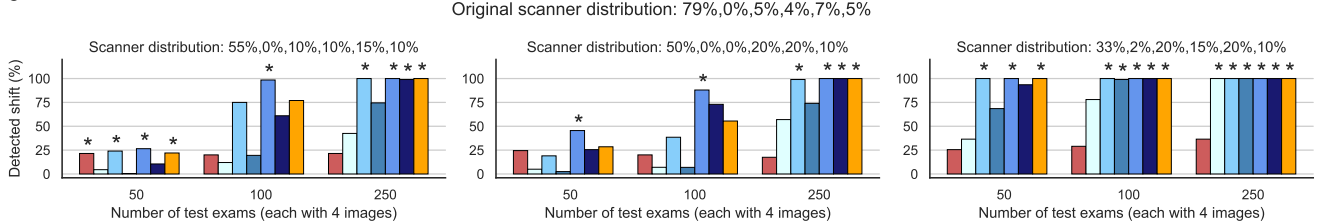
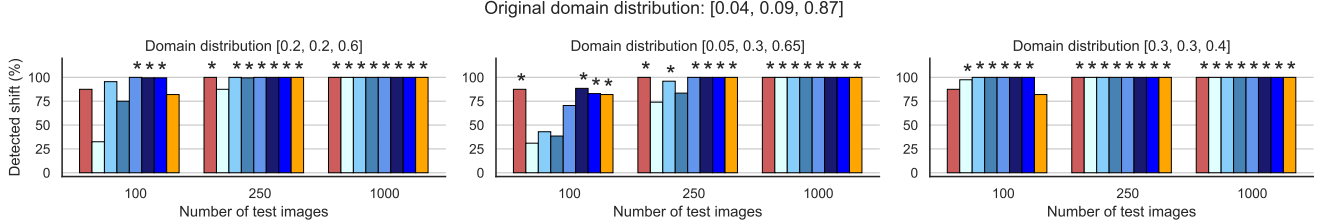
we look at acquisition or subpopulation shifts (see Fig. 4). For these shifts, most feature-based detectors perform substantially better than output-based detectors. Output-based shift detection fails to detect gender shifts on radiography datasets (less than 5% of shifts detected) and performs substantially worse than feature-based tests on acquisition shifts across all levels of shifts and datasets. For example, on EMBED with 250 test exams, the output-based shift detector only detects 25% of acquisition shifts, whereas feature-based detectors detect at least 80% of shifts (except for the random encoder). In Appendix Fig. 2 we report the false shift detection rate of shift detectors when generating test sets without shifts.

**Self-supervised encoders can detect subtle covariate shifts.** Our results show that the effectiveness of feature-based dataset shift detectors is highly dependent on the choice of the encoder used to extract the features (see differences between feature-based detection rates in shades of blue in Fig. 4). The results indicate that for optimal detection of more subtle shifts (e.g. gender shifts), it is important to use an encoder trained in a self-supervised manner. The task model, for example, under-performs for gender shift detection on chest radiography datasets, and so does the encoder trained in a supervised manner on ImageNet data, particularly visible for milder shifts and smaller test set sizes. For example, both supervised encoders fail to detect the shift from 44% to 25% of females in the RSNA dataset, even with large test sizes (Fig. 4 a). Encoders trained in a self-supervised manner (SSL ImageNet and SSL Modality Specific) detect gender shifts with significantly higher sensitivity, exhibiting an average sensitivity of 85% across all gender shifts with a test set size of 250 and 100% for a test set size of 1000. Similarly, for acquisition shifts, results show that SSL encoders offer substantially better detection rates than their supervised counterparts. The SSL model trained on ImageNet data was particularly effective and, in some cases, even better than the modality-specific SSL models for PadChest and EMBED, especially for subtle shifts and in the low test data regime. On the RETINA dataset, self-supervised encoders also all outperform their supervised counterparts, with no significant differences between self-supervised encoders.

**Combining output- and feature-based detection.** Building on the previous findings, we introduce a dual detection approach combining responses from output-based and feature-based shift detectors, using self-supervised features for more robust shift detection. Results in Figs. 3 and 4 demonstrate that the proposed 'Duo' detector (in orange) performs best overall across shifts and datasets, regardless of the shift severity. For example, with the duo detector and test set size of 1000 samples, the detection accuracy is > 80% for nearly every shift, across all datasets. On the contrary, the other detectors respectively fail either on prevalence shift (with feature-based detectors detecting less than 50% prevalence shift cases averaged over datasets) or on covariate shift (where output-based detection detects less than 5% of gender shifts for radiography and less than 25% of acquisition shifts for EMBED). We employ



**Fig. 3 Prevalence shift: shift detectors comparison.** We report the shift detection rate over 200 bootstrap samples. Results show that output-based detection is best for detecting prevalence shifts. For each combination of test set size and type of shift, the detector with the highest detection rate, as well as all detectors not significantly different from the best, are denoted with an asterisk \*.

**a****b****c****d****e****Shift detector**

■ Output-based (task model)	■ Feature-based (Supervised ImageNet)	■ Feature-based (SSL ImageNet)	■ Feature-based (Retfound)
■ Feature-based (Random encoder)	■ Feature-based (Task model)	■ Feature-based (SSL Modality Specific)	■ Feature-based (Duo (model output + SSL ImageNet features))

**Fig. 4 Covariate shifts: shift detectors comparison.** We studied two sub-types of covariate shifts: subpopulation shift (a-b) and acquisition shift (c-e). We report the shift detection rate over 200 bootstrap samples. Results show that feature-based detection is best for this type of shift. For each combination of test set size and type of shift, the detector with the highest detection rate, as well as all detectors not significantly different from the best, are denoted with an asterisk \* .

this dual approach for the detection module of our shift identification pipeline.

## Shift identification performance

To perform shift identification, we leverage the fact that output-based and feature-based shift measures detect different types of shifts to precisely identify the shift present in the test dataset, following a decision logic detailed in Methods [Dataset shift identification](#) and illustrated in Fig. 2.

In-depth evaluation results in Figs. 5 and 6 demonstrate that our novel shift identification framework is capable of distinguishing between prevalence shifts, covariate shifts and mixed shifts with high accuracy across all datasets and types of shifts. Overall, more subtle shifts are best detected with larger test sets whereas larger shifts can be detected with smaller test sets. For prevalence shifts, the average shift identification rate, across datasets and shift levels, is 85% with 500 test images and reaches 95% with 1,000 test images (Fig. 5 a-d). Similarly, for covariate shifts caused by acquisition shifts, when using a test set size of 500 images (and 250 test exams on EMBED), the identification accuracy is greater than 80% for any shift level and dataset, with an average identification accuracy of 89% across datasets and shift levels (Fig. 5 g-i). For the RETINA dataset, identification rates already reach 100% with a test set as small as 250 images. When the covariate shift is induced by gender shifts, covariate shift is detected with identification accuracies greater than 90% for both PadChest and RSNA Pneumonia, with a test set size of 500 images, for all but one shift level (Fig. 5 e-f). Results in Fig. 6, show that the framework is also able to accurately distinguish between cases of covariate shift only and cases of covariate and prevalence shifts. For these mixed shifts, shifts are identified with increasingly high accuracy as the test set size increases. With a test set of 1,000 images, mixed gender and prevalence shifts are correctly identified as mixed shifts with an average accuracy of 97% for RSNA Pneumonia and 75% for PadChest. Mixed shifts induced by acquisition and prevalence shifts are detected with an average 100% accuracy for the RETINA dataset, 77% for PadChest and 79% for EMBED, across shift levels with 1,000 test images. The overall identification accuracy for mixed shifts across all shifts and datasets is 85% (with 1000 test images).

## Discussion

Shift identification is critical for root cause analysis of AI performance drift. We propose a lightweight and practical shift identification framework, capable of detecting and identifying important real-world dataset shifts. Our results show that the proposed framework separates prevalence shifts from covariate shifts with high accuracy, as well as identifies cases of mixed shifts, across three different data modalities and various types of realistic shifts. By analysing common dataset shift detection paradigms, we find that different types of shifts require different types of shift detectors. Our analysis also demonstrates the importance of the choice of encoders for feature-

based dataset shift detection. In particular, we find that encoders trained in a self-supervised manner yield features with substantially higher shift detection power than supervised counterparts. Maybe surprisingly, our results show that generic encoders trained in a self-supervised manner on natural images (ImageNet) provide highly discriminative features for medical image dataset shift detection, transportable across datasets. Following these findings, we evaluate a new dual dataset shift detector, combining shift detection signals from task model outputs tests and features from self-supervised encoders. This approach outperforms existing shift detectors. The consistency of shift detection performance across various types of shifts is crucial as the nature of the shift is, by definition, unknown at test time. We take this combined approach a step further to perform fine-grained shift identification, showing high accuracy in correctly identifying the type of shift present in the test set across all modalities, tasks and various levels of shift intensity. Our results demonstrate the practical value of the shift identification method, which does not require any training at test time, nor any ground truth labels or annotations on the test domain data. The use of a readily available self-supervised encoder trained on ImageNet data for feature extraction dispenses us from training any additional model for shift detection and identification purposes. Combining signals from both feature-based and model output-based shift detectors yields reliable and consistent detection and identification across all types of shifts. Importantly, our method not only separates covariate shifts from prevalence shifts but also reliably detects when both types of shifts are present in the test set, rendering the proposed method applicable to many real-world deployment scenarios.

In practice, the proposed framework can be used as a continuous monitoring tool for any image-based, clinical AI model. Similar to other continuous monitoring tools<sup>4,38</sup>, the shift identification framework would run on the stream of incoming data, collecting test data on a rolling time window. The reference data should be a small dataset representative of the expected data distribution on which the model has been validated. Our results show that with at most 2000 reference images, a test set of only 500 images suffices to yield high shift detection and identification accuracy across all shifts and datasets (> 80%).

In terms of limitations, we note that in the case of covariate shift, on its own, the proposed shift identification framework does not allow for a more fine-grained identification of the origin of shift, e.g. the distinction between population and acquisition shifts. To allow for an even more precise sub-type shift identification, integrating metadata statistics in the pipeline (e.g. as in multi-modal shift detection pipelines<sup>38</sup>) could complement the framework. Nevertheless, it is important to highlight that relying solely on metadata monitoring only enables the detection of shifts affecting the specific attributes collected at test time. For example, statistics on patient population, such as age distribution, gender distribution, may be recorded at deployment time and used to detect *some* sub-types of shifts. Should the metadata not be available at test time, one could use auxiliary models to predict attributes of interest from images directly (e.g. ethnicity<sup>39</sup>). However, solely relying on collected (or pre-

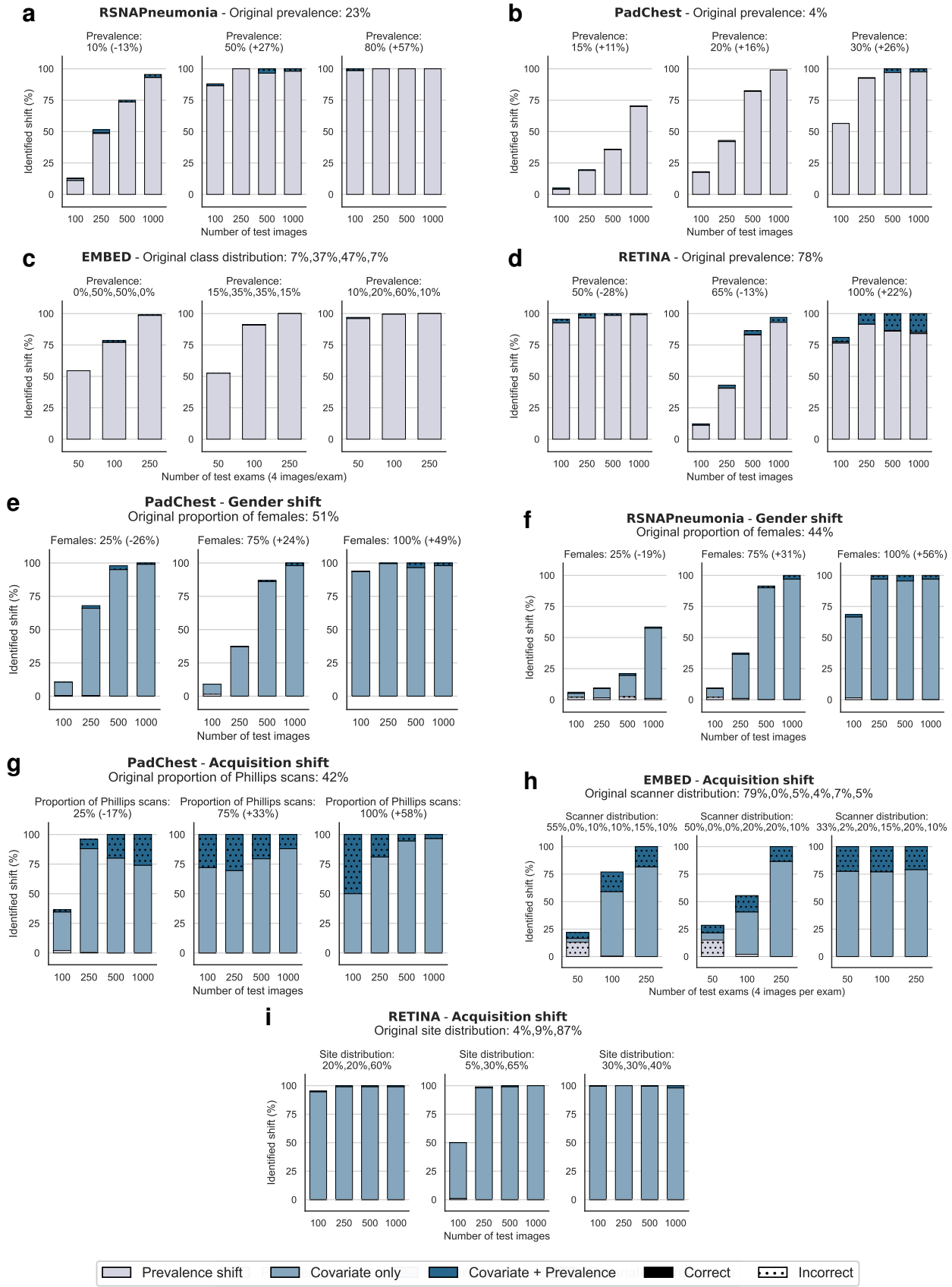


**Fig. 5 Shift identification accuracy: prevalence shifts (a-d) and covariate shifts (e-i).** Across all datasets, the shift identification framework is able to successfully detect and identify both prevalence shifts and covariate shifts with high accuracy. Identification accuracy is computed over 200 bootstrap samples.

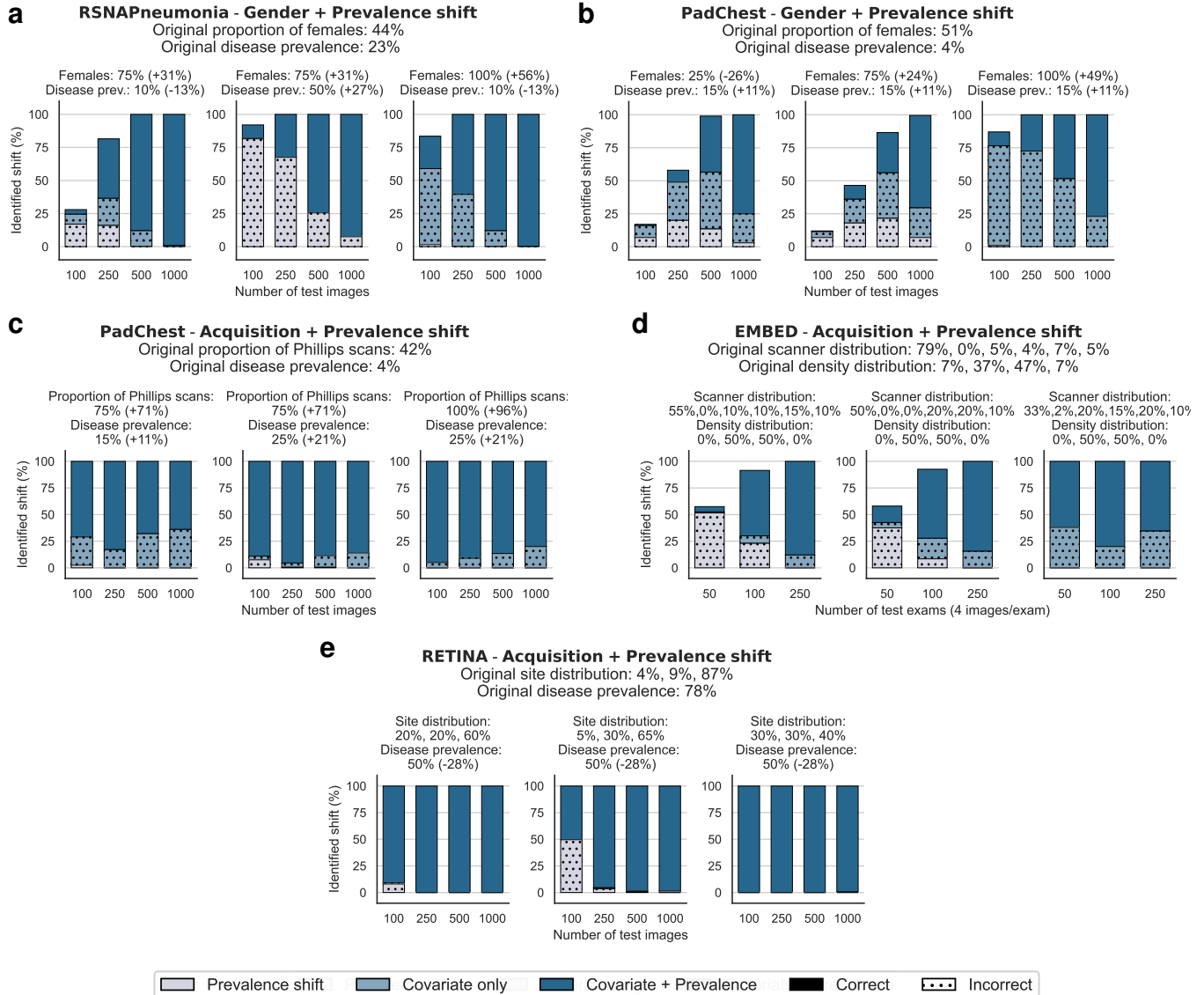


**Fig. 6 Shift identification accuracy: mixed covariate and prevalence shifts.** (a-b) depicts mixed gender and prevalence shift, (c-e) show mixed acquisition and prevalence shift. Across all datasets, the shift identification framework is able to successfully detect and identify presence of both shifts with high accuracy. Identification accuracy is computed over 200 bootstrap samples.

dicted) metadata may not capture all sources of covariate shifts and will not allow detection of prevalence shift. The proposed framework can help uncover shifts that are not detectable by means of simply tracking population metadata. Shift detection and identification can prompt further investigation and inform root cause analysis of AI performance degradation. In this context, our shift identification framework offers an important safeguard for deploying AI models in clinical practice.

## Methods

### Definitions of prevalence and covariate shift

Formally, let  $X$  denote the input image and  $Y$  denote the target (e.g. disease label). *Label shift* (or prevalence shift) occurs when  $P_{ref}(Y) \neq P_{test}(Y)$ , where  $P_{ref}(Y)$  is the distribution of labels on the reference domain and  $P_{test}(Y)$  on the test domain. Label shift<sup>40</sup> assumes that the conditional distributions as well the marginal input distributions are preserved, i.e.  $P_{ref}(X|Y) = P_{test}(X|Y)$  and  $P_{ref}(X) = P_{test}(X)$ . Conversely, *covariate shift* occurs when  $P_{ref}(X) \neq P_{test}(X)$ , while the conditional distributions  $P_{ref}(Y|X)$  and  $P_{test}(Y|X)$  are preserved<sup>40</sup>. Acquisition and subpopulation shifts are both cases of covariate shifts as they directly affect image appearance, i.e. marginal data densities.

### Dataset shift detection methods

Several paradigms have been proposed for dataset shift detection. The most widely used and simplest method to implement consists of comparing distributions of a classifier's outputs between the reference and test domain, proposed by Rabanser et al.<sup>19</sup> and referred to as 'Black Box Shift Detection' (BBSD). Specifically, softmax model outputs (predicted probabilities) are collected for all samples in the reference and test sets. Then, for each class, a separate univariate Kolmogorov-Smirnov (KS) test is run to determine if the class-wise predicted probabilities distributions differ between reference and test domain. A multiple-testing Bonferroni<sup>41</sup> correction is then applied to the individual tests to determine the overall significance of the test.

In the same study, Rabanser et al.<sup>19</sup> also propose another type of shift detector where reference and test data input distribution are compared using a feature-based approach. In this test, the input sample (image) first gets projected to a smaller dimension, e.g. through a pretrained neural network encoder and the shift is then measured using the 'Maximum Mean Discrepancy' permutation test originally proposed by<sup>42</sup>. The Maximum Mean Discrepancy measures the distance between two distributions  $p$  and  $q$  based on the distance between their mean embeddings. An unbiased estimate of the square of the MMD

statistic can be computed via

$$\widehat{MMD} = \frac{1}{m^2 - m} \sum_{i=1}^m \sum_{j \neq i}^m \kappa(z_i, z_j) + \frac{1}{n^2 - n} \sum_{i=1}^n \sum_{j \neq i}^n \kappa(z'_i, z'_j) - \frac{2}{mn} \sum_{i=1}^m \sum_{j=1}^n \kappa(z_i, z'_j),$$

where  $\{z_i\}_{i=1}^m \sim p$ , and  $\{z'_i\}_{i=1}^n \sim q$  and  $\kappa$  is a kernel over the embedding space. The p-value can then be obtained using a permutation test. In Rabanser et al. they proposed to use the RBF kernel  $\kappa(z, \tilde{z}) = e^{\frac{1}{\sigma} \|z - \tilde{z}\|^2}$ , setting  $\sigma$  as the median distance between all samples. An alternative way would be to explicitly learn the kernel<sup>43</sup> with 'deep kernels'. The disadvantage of this approach is that the kernel needs to be learned for every single test set for which one wishes to run shift detection. In this work, we use the RBF kernel.

Additionally, we propose and evaluate a dual shift detector, combining BBSD and MMD outcomes (referred to as 'Duo'). We first run each test independently, this yields  $C$  p-values for the BBSD test (one per class), and one p-value for the MMD permutation test. To account for multiple testing, we then apply Bonferroni correction<sup>41</sup> on the  $C + 1$  p-values to get the overall dual test outcome.

Another existing shift detection approach consists of training a domain classifier to classify samples between the reference and test domains<sup>44-46</sup> and using the accuracy of this classifier as a proxy for measuring distances between distributions. One drawback of this approach is its high computational cost: for every test set, a new domain classifier must be trained, which is highly impractical in continuous monitoring scenarios. Hence, we here focus on output-based (BBSD) and feature-based (MMD) shift detection methods, as these do not require training of additional models at test-time.

### Dataset shift identification

In this work, we propose a novel framework for identifying whether dataset shift is caused by prevalence shift, by covariate shift or by a mix of both. The process is summarised in Fig. 2. The approach can be divided into two stages. In the first step, we perform 'standard' dataset shift detection to separate the 'shift' from the 'no shift' cases. For this detection step, we use the proposed dual detection approach, combining signals from model outputs and self-supervised features to detect shifts (see **Dataset shift detection methods**). Provided that a shift has been detected in this first step, we add an additional 'shift identification' step to separate prevalence from covariate shifts. We start by estimating the label distribution in the test dataset using the density ratio estimator from state-of-the-art label adaptation method CPMCN<sup>22</sup> (see next section). Next, we undersample the reference set to match the estimated test set prevalence shift. We then compare feature distributions between the prevalence-adjusted reference set and the test set. If adjusting

the prevalence removes all significant differences between the reference and test set, the shift is attributed to prevalence shift. Otherwise, covariate shift is necessarily present. Finally, given that a covariate shift has been detected, we need to determine whether a prevalence shift is also present (mixed shift). To answer this question, we leverage the fact that model output-based and feature-based detectors exhibit different behaviours in function of the type of shifts. In particular, our analysis of shift detection methods showed that model output-based shift detection is best suited for prevalence shift detection. Hence, we compare model output distributions to separate cases of covariate shift only from cases of mixed shifts. Precisely, if output distributions were significantly different before adjusting the prevalence on the reference set, but differences disappear after adjusting the prevalence, we conclude that prevalence shift is also responsible for the observed shift, hence the observed shift is a mix of prevalence and covariate shift (mixed shift). Else, the shift is attributed to ‘covariate shift’ only.

## Prevalence shift estimation and adaptation

Many studies have proposed algorithms to alleviate the detrimental effect of prevalence shift on machine learning models. Most methods follow the same over-arching idea: (i) estimate the density ratio  $P_{ref}(Y)/P_{test}(Y)$ ; (ii) use this ratio to recalibrate the model<sup>14,22,23,47</sup>. In this work, we are primarily interested in the first step, to estimate the prevalence in the test set in the absence of labels. Various methods have been proposed to estimate this density ratio, mostly differing by their computational costs<sup>14,22,23,47</sup>. Here, we use the recently proposed state-of-the-art ‘class probability matching with calibration network’ (CPMCN) method by Wen et al.<sup>22</sup> to estimate this ratio. In this work, the authors estimate the density ratio  $w \in \mathbb{R}^C$ , with  $w_i = \frac{P_{test}(Y=i)}{P_{ref}(Y=i)}$  by

$$\hat{w} := \arg \min_{w \in \mathbb{R}^C} \sum_{i=1}^C \left| \hat{P}_{ref}(Y=i) - \frac{1}{m} \sum_{x \in D_t} \frac{\hat{p}(i|x)}{\sum_j^C w_j \hat{p}(j|x)} \right|^2$$

with  $m$  the number of samples in the test set  $D_t$ ,  $\hat{P}_{ref}(Y=i)$  is the empirical proportion of samples with class  $i$  in the reference set, and  $\hat{p}(i|x)$  is the probability predicted by the model for class  $i$  given sample  $x$ . Given this estimated ratio  $\hat{w}$ , we can easily recover the estimated label distribution on the test domain

$$\hat{P}_{test}(Y=i) = \hat{w}_i \cdot \hat{P}_{ref}(Y=i), \forall i \in C$$

We follow this method to estimate the label distribution in the test set in our shift identification module.

Note that, once the density ratio has been estimated, it can be used to recalibrate model outputs to mitigate the effects of prevalence shifts on model performance. Precisely, re-calibrated probabilities can be computed by:

$$\hat{q}(i|x) = \frac{\hat{w}_i \hat{p}(i|x)}{\sum_{j=1}^m \hat{w}_j \hat{p}(j|x)} \quad (1)$$

where  $\hat{p}(i|x)$  are the original model outputs and  $\hat{q}(i|x)$  the re-calibrated output, for sample  $x$  and class  $i$ .

## Self-supervised learning

Self-supervised learning aims to learn meaningful representations of images without relying on labelled data<sup>21,48,49</sup>. Two prominent paradigms for learning such representations are contrastive learning and predictive coding methods. In contrastive learning, models are trained to learn similar representations for semantically related pairs of image *views* (positive pairs) while pushing them away from the representations of unrelated inputs (negative pairs). A seminal work in this area is SimCLR<sup>21</sup>, where different views are created using heavy random data augmentation pipelines and representations are optimised using a normalised temperature-scaled cross-entropy loss<sup>21</sup>. SimCLR has since been refined in numerous follow-up studies<sup>48,50-52</sup>, yet remains widely used. On the other hand, predictive coding approaches, such as Masked Auto Encoders<sup>49</sup>, learn representations by masking parts of the input and training a neural network to reconstruct the missing regions, encouraging the network to build a fine-grained understanding of the semantic information present in the visible parts of the image.

## Datasets

For chest radiography, we use two public datasets for our analysis: the RSNA Pneumonia dataset<sup>31</sup>, a subset of the NIH Chest-Xray8 dataset<sup>53</sup> manually relabelled by expert radiologists for presence of pneumonia-like opacities. We use the original metadata from the NIH Chest-Xray8 dataset<sup>53</sup> to retrieve patient gender. We also use PadChest<sup>30</sup> a larger dataset containing multiple disease labels extracted from radiology reports. We here focus on the pneumonia label. Importantly, this dataset contains important metadata such as scanner information or the gender of the patient, allowing us to generate a wide range of shifts. For mammography, we use the EMBED dataset<sup>32</sup> a large mammogram dataset collected in the US, on 6 different scanners. Finally, for fundus imaging, we create ‘RETINA’ a multi-domain dataset by combining three different public datasets: the Kaggle Diabetic Retinopathy Detection<sup>33</sup> dataset, the Kaggle Aptos Blindness Detection dataset<sup>34</sup> and the Messidor-v2 dataset<sup>35</sup>. These datasets cover different regions of the world (India, France, US) but also with varying image acquisition devices: images from the Messidor-v2 are high-quality images, while many images in the Kaggle datasets are of lower quality (including phone pictures). Creating this multi-centre dataset allows us to simulate various domain shifts by varying the proportion of data from each ‘site’ (original dataset source). The task of interest for fundus images here is binary diabetic retinopathy (DR) classification for fundus images, where we classify images between referable DR (grades 2,3,4) and healthy/non-referable DR (grades 0,1).

## Shift generation details

For prevalence shifts, we assume that the task of interest is pneumonia detection for chest x-ray images, breast density classification for mammography and binary diabetic retinopathy classification for fundus images. In terms of covariate shifts, we simulate different sub-types of shifts depending on the datasets at hand. For both chest radiography datasets, we first simulate sub-population shift in the form of gender shift where we vary the proportion of female patients in the test set. PadChest<sup>30</sup> additionally includes scanner labels, allowing the study of acquisition shift. The dataset features scans from two types of scanners, 'Phillips' and 'Imaging', with an initial 40%-60% distribution. To simulate different levels of acquisition shift, we vary the proportion of Phillips scans in the test set. Similarly, for the EMBED<sup>32</sup> mammography dataset, we simulate various levels of acquisition shift by varying the distribution of scanners in the test set. This dataset offers a complementary view to the chest x-ray datasets, addressing a multi-class problem (unlike the binary pneumonia detection task) and providing even more flexibility for simulating diverse levels of acquisition shifts (as it contains data from six different scanners). Note that in EMBED each standard mammography exam comprises 4 mammograms (left/right breasts and MLO/CC views). We excluded all exams that did not contain exactly four images and kept exactly one exam per patient. For this dataset, test set resampling was done at the exam level (as opposed to image-level sampling for other datasets). Finally, for our RETINA dataset, we simulate domain shifts by varying the proportion of samples coming from each underlying dataset (Aptos<sup>34</sup>, Kaggle DR<sup>33</sup> and Mesidor<sup>35</sup>).

## Implementation details

For all datasets, we first define train, validation and test splits. The training set is reserved for training task models (pneumonia, density and DR classification). All task models are ResNet-50 models initialised with ImageNet weights. To evaluate the shift identification accuracy of the proposed frameworks, we follow standard evaluation practices from the dataset shift detection literature. Specifically, we repeat the following process 200 times: (i) sample a subset of size  $N_{test}$  from the original test split according to the shift of interest, (ii) run the shift identification test, and (iii) record whether the shift is correctly identified. The final shift identification accuracy is computed as the proportion of times the shift is correctly identified out of the bootstrap samples. For each bootstrap repetition, we also re-sample the reference set (against which we measure the shift) by taking a random sample of  $N_{ref}$  data points from the validation set (uniformly at random). For both chest radiography datasets, we used  $N_{ref} = 2,000$  images and  $N_{test} \in \{100, 250, 500, 1000\}$  images. For the RETINA dataset, we used  $N_{ref} = 1,000$  images and  $N_{test} \in \{100, 250, 1000\}$  images. The case of EMBED is slightly different as we need to ensure that images belonging to the same exam are always sampled simultaneously. Hence, for this dataset sampling of all the reference sets, shifted test sets (and permutations in the MMD

test<sup>1</sup>) is done at the exam level and not at the image level. We assumed  $N_{exams,ref} = 1,000$  exams (i.e 4,000 images) and  $N_{exams,test} \in \{50, 100, 250\}$ .

For each dataset, we use the task model for the BBSD test. For the MMD detection test, we first extract the embeddings from the last layer of the encoder, then project them onto the 32-first principle components and then use the RBF kernel (see [Dataset shift detection methods](#)). We compare various encoders for feature extraction, in particular encoders trained in a self-supervised manner. Self-supervised encoders were trained using the SimCLR<sup>21</sup> objective, with a ResNet-50<sup>55</sup> architecture. Additionally, for the RETINA dataset, we compare with RetFound<sup>37</sup> a publicly available self-supervised foundation model trained with the Masked Auto Encoder objective on a large set of retinal images, based on a transformer architecture (ViT<sup>56</sup>). All the code necessary to reproduce our experiments is made publicly available.<sup>2</sup>.

## References

1. K. Zhou, Z. Liu, Y. Qiao, T. Xiang, and C. C. Loy, "Domain Generalization: A Survey," *IEEE Transactions on Pattern Analysis and Machine Intelligence*, vol. 45, pp. 4396–4415, Apr. 2023. Conference Name: IEEE Transactions on Pattern Analysis and Machine Intelligence.
2. L. Garrucho, K. Kushibar, S. Jouide, O. Diaz, L. Igual, and K. Lekadir, "Domain generalization in deep learning based mass detection in mammography: A large-scale multi-center study," *Artificial Intelligence in Medicine*, vol. 132, p. 102386, Oct. 2022.
3. S. Garg, N. Erickson, J. Sharpnack, A. Smola, S. Balakrishnan, and Z. C. Lipton, "RLSbench: Domain Adaptation Under Relaxed Label Shift," in *Proceedings of the 40th International Conference on Machine Learning*, pp. 10879–10928, PMLR, July 2023.
4. M. Roschewitz, G. Khara, J. Yearsley, N. Sharma, J. J. James, E. Ambrozay, A. Heroux, P. Kecskemethy, T. Rijken, and B. Glocker, "Automatic correction of performance drift under acquisition shift in medical image classification," *Nature Communications*, vol. 14, p. 6608, Oct. 2023.
5. D. C. Castro, I. Walker, and B. Glocker, "Causality matters in medical imaging," *Nature Communications*, vol. 11, p. 3673, July 2020. Publisher: Nature Publishing Group.
6. P. Godau, P. Kalinowski, E. Christodoulou, A. Reinke, M. Tizabi, L. Ferrer, P. F. Jäger, and L. Maier-Hein, "Deployment of Image Analysis Algorithms Under Prevalence Shifts," in *Medical Image Computing and Computer Assisted Intervention – MICCAI 2023: 26th International Conference, Vancouver, BC, Canada, October 8–12, 2023, Proceedings, Part III*, (Berlin, Heidelberg), pp. 389–399, Springer-Verlag, Oct. 2023.

<sup>1</sup>Keeping the underlying structure of the data during permutation tests is important to avoid inflated type I error<sup>54</sup>.

<sup>2</sup><https://anonymous.4open.science/r/shift-id-C7CF/README.md>

7. W. Ma, C. Chen, S. Zheng, J. Qin, H. Zhang, and Q. Dou, “Test-Time Adaptation with Calibration of Medical Image Classification Nets for Label Distribution Shift,” in *Medical Image Computing and Computer Assisted Intervention – MICCAI 2022* (L. Wang, Q. Dou, P. T. Fletcher, S. Speidel, and S. Li, eds.), Lecture Notes in Computer Science, (Cham), pp. 313–323, Springer Nature Switzerland, 2022.
8. W. Yan, L. Huang, L. Xia, S. Gu, F. Yan, Y. Wang, and Q. Tao, “MRI Manufacturer Shift and Adaptation: Increasing the Generalizability of Deep Learning Segmentation for MR Images Acquired with Different Scanners,” *Radiology. Artificial Intelligence*, vol. 2, p. e190195, July 2020.
9. N. Sharma, A. Y. Ng, J. J. James, G. Khara, E. Ambrozay, C. C. Austin, G. Forrai, G. Fox, B. Glocker, A. Heindl, E. Karpati, T. M. Rijken, V. Venkataraman, J. E. Yearsley, and P. D. Kecskemethy, “Multi-vendor evaluation of artificial intelligence as an independent reader for double reading in breast cancer screening on 275,900 mammograms,” *BMC Cancer*, vol. 23, p. 460, May 2023.
10. K. Stacke, G. Eilertsen, J. Unger, and C. Lundstrom, “Measuring Domain Shift for Deep Learning in Histopathology,” *IEEE journal of biomedical and health informatics*, vol. 25, pp. 325–336, Feb. 2021.
11. Y. Appelman, B. B. van Rijn, M. E. ten Haaf, E. Boersma, and S. A. E. Peters, “Sex differences in cardiovascular risk factors and disease prevention,” *Atherosclerosis*, vol. 241, pp. 211–218, July 2015.
12. Y. Yang, H. Zhang, J. W. Gichoya, D. Katabi, and M. Ghassemi, “The limits of fair medical imaging AI in real-world generalization,” *Nature Medicine*, pp. 1–11, June 2024.
13. L. Seyyed-Kalantari, H. Zhang, M. B. A. McDermott, I. Y. Chen, and M. Ghassemi, “Underdiagnosis bias of artificial intelligence algorithms applied to chest radiographs in under-served patient populations,” *Nature Medicine*, vol. 27, pp. 2176–2182, Dec. 2021. Number: 12 Publisher: Nature Publishing Group.
14. A. Alexandari, A. Kundaje, and A. Shrikumar, “Maximum Likelihood with Bias-Corrected Calibration is Hard-To-Beat at Label Shift Adaptation,” in *Proceedings of the 37th International Conference on Machine Learning*, pp. 222–232, PMLR, Nov. 2020. ISSN: 2640-3498.
15. Finlayson Samuel G., Subbaswamy Adarsh, Singh Karandeep, Bowers John, Kupke Annabel, Zittrain Jonathan, Kohane Isaac S., and Saria Suchi, “The Clinician and Dataset Shift in Artificial Intelligence,” *New England Journal of Medicine*, vol. 385, pp. 283–286, July 2021. Publisher: Massachusetts Medical Society eprint: <https://www.nejm.org/doi/pdf/10.1056/NEJMc2104626>.
16. B. Sahiner, W. Chen, R. K. Samala, and N. Petrick, “Data drift in medical machine learning: implications and potential remedies,” *British Journal of Radiology*, vol. 96, p. 20220878, Oct. 2023.
17. L. M. Koch, C. M. Schürch, C. F. Baumgartner, A. Gretton, and P. Berens, “Deep Hypothesis Tests Detect Clinically Relevant Subgroup Shifts in Medical Images,” Mar. 2023. arXiv:2303.04862 [cs].
18. L. M. Koch, C. F. Baumgartner, and P. Berens, “Distribution shift detection for the postmarket surveillance of medical AI algorithms: a retrospective simulation study,” *npj Digital Medicine*, vol. 7, pp. 1–11, May 2024. Publisher: Nature Publishing Group.
19. S. Rabanser, S. Günnemann, and Z. Lipton, “Failing Loudly: An Empirical Study of Methods for Detecting Dataset Shift,” in *Advances in Neural Information Processing Systems*, vol. 32, Curran Associates, Inc., 2019.
20. J. Feng, A. Subbaswamy, A. Gossman, H. Singh, B. Sahiner, M.-O. Kim, G. A. Pennello, N. Petrick, R. Pirracchio, and F. Xia, “Designing monitoring strategies for deployed machine learning algorithms: navigating performativity through a causal lens,” in *Proceedings of the Third Conference on Causal Learning and Reasoning*, pp. 587–608, PMLR, Mar. 2024.
21. T. Chen, S. Kornblith, M. Norouzi, and G. Hinton, “A Simple Framework for Contrastive Learning of Visual Representations,” in *Proceedings of the 37th International Conference on Machine Learning*, pp. 1597–1607, PMLR, Nov. 2020. ISSN: 2640-3498.
22. H. Wen, A. Betken, and H. Hang, “Class Probability Matching with Calibrated Networks for Label Shift Adaptation,” in *Proceedings of The Twelfth International Conference on Learning Representations*, Apr. 2024.
23. M. Saerens, P. Latinne, and C. Decaestecker, “Adjusting the Outputs of a Classifier to New a Priori Probabilities: A Simple Procedure,” *Neural Computation*, vol. 14, pp. 21–41, Jan. 2002.
24. Z. Lipton, Y.-X. Wang, and A. Smola, “Detecting and Correcting for Label Shift with Black Box Predictors,” in *Proceedings of the 35th International Conference on Machine Learning*, pp. 3122–3130, PMLR, July 2018.
25. L. Zuo, B. E. Dewey, Y. Liu, Y. He, S. D. Newsome, E. M. Mowry, S. M. Resnick, J. L. Prince, and A. Carass, “Unsupervised MR harmonization by learning disentangled representations using information bottleneck theory,” *NeuroImage*, vol. 243, p. 118569, Nov. 2021.
26. S. Cao, N. Konz, J. Duncan, and M. A. Mazurowski, “Deep Learning for Breast MRI Style Transfer with Limited Training Data,” *Journal of Digital Imaging*, vol. 36, pp. 666–678, Apr. 2023.
27. H. Kang, D. Luo, W. Feng, S. Zeng, T. Quan, J. Hu, and X. Liu, “StainNet: A Fast and Robust Stain Normalization Network,” *Frontiers in Medicine*, vol. 8, 2021.
28. S. Xie, Z. Zheng, L. Chen, and C. Chen, “Learning Semantic Representations for Unsupervised Domain Adaptation,” in *Proceedings of the 35th International Conference on Machine Learning*, pp. 5423–5432, PMLR, July 2018. ISSN: 2640-3498.
29. Y. Yang, H. Zhang, D. Katabi, and M. Ghassemi, “Change is hard: a closer look at subpopulation shift,” in *Proceedings of the 40th International Conference on Machine Learning*, vol. 202 of *ICML’23*, (Honolulu, Hawaii, USA), pp. 39584–39622, JMLR.org, July 2023.

30. A. Bustos, A. Pertusa, J.-M. Salinas, and M. de la Iglesia-Vayá, “PadChest: A large chest x-ray image dataset with multi-label annotated reports,” *Medical Image Analysis*, vol. 66, p. 101797, Dec. 2020.

31. G. Shih, C. C. Wu, S. S. Halabi, M. D. Kohli, L. M. Prevedello, T. S. Cook, A. Sharma, J. K. Amorosa, V. Arteaga, M. Galperin-Aizenberg, R. R. Gill, M. C. Godoy, S. Hobbs, J. Jeudy, A. Laroia, P. N. Shah, D. Vumidi, K. Yaddanapudi, and A. Stein, “Augmenting the National Institutes of Health Chest Radiograph Dataset with Expert Annotations of Possible Pneumonia,” *Radiology: Artificial Intelligence*, vol. 1, p. e180041, Jan. 2019. Publisher: Radiological Society of North America.

32. J. J. Jeong, B. L. Vey, A. Bhimireddy, T. Kim, T. Santos, R. Correa, R. Dutt, M. Mosunjac, G. Oprea-Ilies, G. Smith, M. Woo, C. R. McAdams, M. S. Newell, I. Banerjee, J. Gichoya, and H. Trivedi, “The EMory BrEast imaging Dataset (EMBED): A Racially Diverse, Granular Dataset of 3.4 Million Screening and Diagnostic Mammographic Images,” *Radiology: Artificial Intelligence*, vol. 5, p. e220047, Jan. 2023. Publisher: Radiological Society of North America.

33. E. Dugas, J. Jared, and W. Cukierski, “Diabetic Retinopathy Detection Kaggle Challenge,” 2015.

34. M. Karthik and D. Sohier, “APTOPS 2019 Blindness Detection Kaggle Challenge,” 2019.

35. E. Decencière, X. Zhang, G. Cazuguel, B. Lay, B. Cochener, C. Trone, P. Gain, R. Ordóñez, P. Massin, A. Erginay, B. Charton, and J.-C. Klein, “Feedback on a publicly distributed image database: the messidor database,” *Image Analysis and Stereology*, vol. 33, pp. 231–234, Aug. 2014. Number: 3.

36. G. Zamzmi, K. Venkatesh, B. Nelson, S. Prathapan, P. Yi, B. Sahiner, and J. G. Delfino, “Out-of-Distribution Detection and Radiological Data Monitoring Using Statistical Process Control,” *Journal of Imaging Informatics in Medicine*, Sept. 2024.

37. Y. Zhou, M. A. Chia, S. K. Wagner, M. S. Ayhan, D. J. Williamson, R. R. Struyven, T. Liu, M. Xu, M. G. Lozano, P. Woodward-Court, Y. Kihara, A. Altmann, A. Y. Lee, E. J. Topol, A. K. Denniston, D. C. Alexander, and P. A. Keane, “A foundation model for generalizable disease detection from retinal images,” *Nature*, vol. 622, pp. 156–163, Oct. 2023. Publisher: Nature Publishing Group.

38. J. Merkow, A. Soin, J. Long, J. P. Cohen, S. Saligrama, C. Bridge, X. Yang, S. Kaiser, S. Borg, I. Tarapov, and M. P. Lungren, “CheXstray: A Real-Time Multi-Modal Monitoring Workflow for Medical Imaging AI,” in *Medical Image Computing and Computer Assisted Intervention – MICCAI 2023* (H. Greenspan, A. Madabhushi, P. Mousavi, S. Salcudean, J. Duncan, T. Syeda-Mahmood, and R. Taylor, eds.), (Cham), pp. 326–336, Springer Nature Switzerland, 2023.

39. J. W. Gichoya, I. Banerjee, A. R. Bhimireddy, J. L. Burns, L. A. Celi, L.-C. Chen, R. Correa, N. Dullerud, M. Ghassemi, S.-C. Huang, P.-C. Kuo, M. P. Lungren, L. J. Palmer, B. J. Price, S. Purkayastha, A. T. Pyrros, L. Oakden-Rayner, C. Okechukwu, L. Seyyed-Kalantari, H. Trivedi, R. Wang, Z. Zaiman, and H. Zhang, “AI recognition of patient race in medical imaging: a modelling study,” *The Lancet Digital Health*, vol. 4, pp. e406–e414, June 2022. Publisher: Elsevier.

40. K. P. Murphy, *Probabilistic Machine Learning: Advanced Topics*. MIT Press, 2023.

41. O. J. Dunn, “Multiple Comparisons among Means,” *Journal of the American Statistical Association*, vol. 56, pp. 52–64, Mar. 1961. Publisher: Taylor & Francis.

42. A. Gretton, K. M. Borgwardt, M. J. Rasch, B. Schölkopf, and A. Smola, “A kernel two-sample test,” *The Journal of Machine Learning Research*, vol. 13, pp. 723–773, Mar. 2012.

43. F. Liu, W. Xu, J. Lu, G. Zhang, A. Gretton, and D. J. Sutherland, “Learning Deep Kernels for Non-Parametric Two-Sample Tests,” in *Proceedings of the 37th International Conference on Machine Learning*, pp. 6316–6326, PMLR, Nov. 2020. ISSN: 2640-3498.

44. X. Cheng and A. Cloninger, “Classification Logit Two-Sample Testing by Neural Networks for Differentiating Near Manifold Densities,” *IEEE Transactions on Information Theory*, vol. 68, pp. 6631–6662, Oct. 2022.

45. D. Lopez-Paz and M. Oquab, “Revisiting Classifier Two-Sample Tests,” in *International Conference on Learning Representations*, July 2022.

46. S. Jang, S. Park, I. Lee, and O. Bastani, “Sequential Covariate Shift Detection Using Classifier Two-Sample Tests,” in *Proceedings of the 39th International Conference on Machine Learning*, pp. 9845–9880, PMLR, June 2022. ISSN: 2640-3498.

47. K. Zhang, B. Schölkopf, K. Muandet, and Z. Wang, “Domain Adaptation under Target and Conditional Shift,” in *Proceedings of the 30th International Conference on Machine Learning*, 2013.

48. M. Oquab, T. Darcret, T. Moutakanni, H. V. Vo, M. Szafraniec, V. Khalidov, P. Fernandez, D. Haziza, F. Massa, A. El-Nouby, M. Assran, N. Ballas, W. Galuba, R. Howes, P.-Y. Huang, S.-W. Li, I. Misra, M. Rabbat, V. Sharma, G. Synnaeve, H. Xu, H. Jegou, J. Mairal, P. Labatut, A. Joulin, and P. Bojanowski, “DINOv2: Learning Robust Visual Features without Supervision,” *Transactions on Machine Learning Research*, July 2023.

49. Y. He, A. Carass, L. Zuo, B. E. Dewey, and J. L. Prince, “Autoencoder based self-supervised test-time adaptation for medical image analysis,” *Medical Image Analysis*, vol. 72, p. 102136, Aug. 2021.

50. M. Caron, I. Misra, J. Mairal, P. Goyal, P. Bojanowski, and A. Joulin, “Unsupervised Learning of Visual Features by Contrasting Cluster Assignments,” in *Advances in Neural Information Processing Systems*, vol. 33, pp. 9912–9924, Curran Associates, Inc., 2020.

51. J.-B. Grill, F. Strub, F. Altché, C. Tallec, P. Richemond, E. Buchatskaya, C. Doersch, B. Avila Pires, Z. Guo, M. Gheshlaghi Azar, B. Piot, k. kavukcuoglu, R. Munos,

and M. Valko, “Bootstrap Your Own Latent - A New Approach to Self-Supervised Learning,” in *Advances in Neural Information Processing Systems*, vol. 33, pp. 21271–21284, Curran Associates, Inc., 2020.

52. K. He, H. Fan, Y. Wu, S. Xie, and R. Girshick, “Momentum Contrast for Unsupervised Visual Representation Learning,” in *2020 IEEE/CVF Conference on Computer Vision and Pattern Recognition (CVPR)*, (Seattle, WA, USA), pp. 9726–9735, IEEE, June 2020.
53. X. Wang, Y. Peng, L. Lu, Z. Lu, M. Bagheri, and R. M. Summers, “ChestX-ray8: Hospital-scale Chest X-ray Database and Benchmarks on Weakly-Supervised Classification and Localization of Common Thorax Diseases,” in *2017 IEEE Conference on Computer Vision and Pattern Recognition (CVPR)*, pp. 3462–3471, July 2017.
54. G. A. Churchill and R. W. Doerge, “Naive Application of Permutation Testing Leads to Inflated Type I Error Rates,” *Genetics*, vol. 178, pp. 609–610, Jan. 2008.
55. K. He, X. Zhang, S. Ren, and J. Sun, “Deep Residual Learning for Image Recognition,” in *2016 IEEE Conference on Computer Vision and Pattern Recognition (CVPR)*, pp. 770–778, IEEE, June 2016.
56. A. Dosovitskiy, L. Beyer, A. Kolesnikov, D. Weissenborn, X. Zhai, T. Unterthiner, M. Dehghani, M. Minderer, G. Heigold, S. Gelly, J. Uszkoreit, and N. Houlsby, “An Image is Worth 16x16 Words: Transformers for Image Recognition at Scale,” in *International Conference on Learning Representations*, Oct. 2020.

## Acknowledgements

M.R. is funded by an Imperial College London President’s PhD Scholarship and a Google PhD Fellowship. R.M. is funded through the European Union’s Horizon Europe research and innovation programme under grant agreement 101080302. C.J. is supported by Microsoft Research and the Engineering and Physical Sciences Research Council (EPSRC) through a Microsoft PhD Scholarship. B.G. acknowledges support from the Royal Academy of Engineering as part of his Kheiron Medical Technologies/RAEng Research Chair in Safe Deployment of Medical Imaging AI and the UKRI AI programme, and the EPSRC, for CHAI - Causality in Healthcare AI Hub [grant number EP/Y028856/1].

## Competing interests

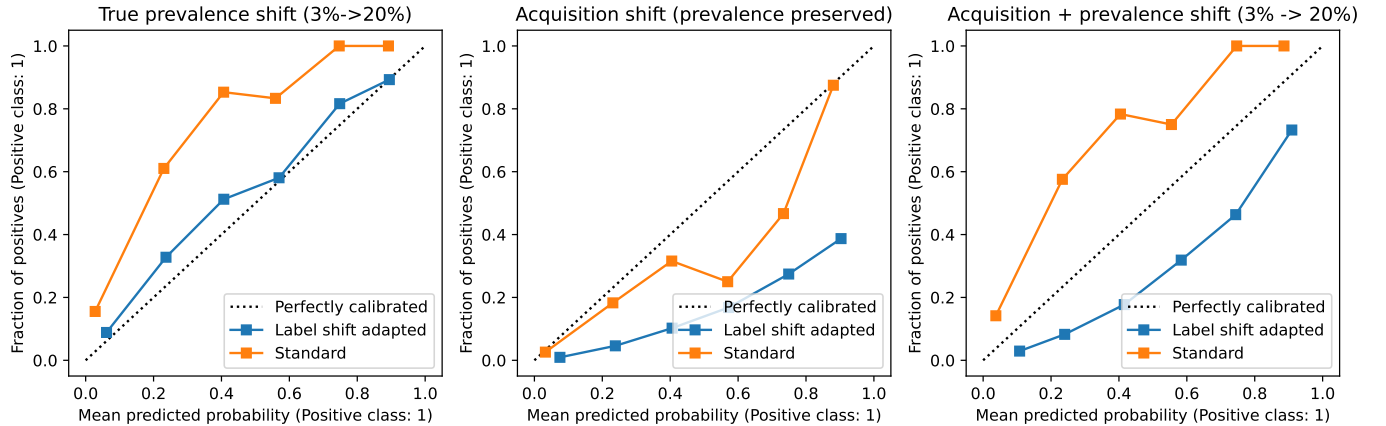
B.G. is a part-time employee of HeartFlow and Kheiron Medical Technologies. All other authors declare no competing interests.

# Supplementary material

## A Appendix A: Motivating example

In this section, our goal is to motivate the need for dataset shift identification, illustrating the usefulness of distinguishing between prevalence shift and covariate shift with a simple example on chest radiography data.

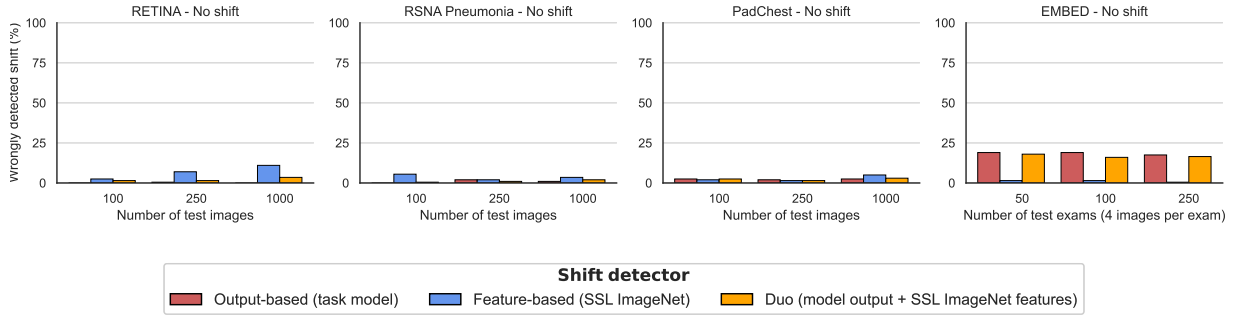
For this motivating example, we use data from the PadChest dataset<sup>30</sup> and focus on classifying images with pneumonia. We then generate various test sets with (i) prevalence shift, (ii) acquisition shift, (iii) both shifts and evaluate the model on these shifted datasets. Our goal is to illustrate why identifying the type of shift occurring is a crucial issue. Indeed, many domain adaptation methods are tailored for specific shifts; label shift adaptation, for example, aims at tackling the effect of prevalence shift only, often explicitly assuming that no other shift is occurring. In supplementary Fig. 1, we show the effect of dataset shift on model calibration before and after applying a post-hoc label shift adaptation algorithm in three settings: (i) only prevalence shift occurs, (ii) acquisition shift occurs instead, (iii) both shifts happen. For prevalence shift, we sampled a test set with 20% prevalence of pneumonia, shifted from the original 3% prevalence in PadChest (training and validation prevalence). For acquisition shift, we create a test set containing 90% of scans taken with Phillips scanner and 10% with Imaging scanner, a shift from the original 40%-60% scanner distribution in PadChest. The label shift adaptation algorithm used for this example is CPMCN<sup>22</sup> (see [Prevalence shift estimation and adaptation](#)). We can clearly see that all shifts cause some amount of model calibration deterioration. More importantly, in the prevalence shift case, CPMCN successfully restores model calibration on the shifted dataset, and the estimated prevalence matches the true test set prevalence. However, for the acquisition shift scenario, the effect of applying label shift correction is counter-productive: calibration is much worse after applying the re-calibration than before. In the case where both shifts are happening at the same time, the re-calibration also fails to restore the calibration. This is, of course, absolutely expected from the theory: label shift adaptation methods like the ones tested here were designed for the case where only prevalence shift is happening. However, this empirical observation confirms the main motivation of our study: *it is crucial to be able to identify the cause of dataset shifts for safe deployment*.



**Supp. Fig. 1** Why dataset shift identification matters: example of wrongly applying label shift adaptation algorithms in scenarios when covariate shift is present. Subplots from left to right show model calibration plots for three scenarios: (i) prevalence shift, (ii) acquisition shift, and (iii) both shifts for a pneumonia detection model on the PadChest dataset. The re-calibration is successful in the prevalence shift only settings but fails (or even harms) in the presence of covariate shift.

## B False detection rate for different shift detectors

In this section, we measure the false detection rate of dataset shift in the absence of shift in the test set generating process. We verify that the false-positive rates of the output-based, feature-based and Duo detectors stay low across datasets and detectors, we find that false detection rates hover around the expected type-I error of the statistical tests 5% for most datasets and detection methods. The only exception is EMBED, where false positive rates are a little higher than expected for the output-based (and hence Duo) detector. This is due to the fact that - for this highly imbalanced classification problem - small randomly resampled test sets may lead to small differences in the observed cumulative distribution of predictions, even in the absence of a shift in the test set generation process.



**Supp. Fig. 2 False detection rate.** Percentage of shift detected when resampling the test set without shift.